Asymmetric Vortex Pair Induces Secondary Traveling Wave Vibration of a Flexible Cylinder from Still Water to Incoming Flow

Zhicheng Wang (王志成)[+,1] Ang Li (李昂)[+,2] Baiheng Wu (仵柏衡)[+,3] Dixia Fan (范迪夏)[*,4,5,6] Michael S. Triantafyllou,[6,7] and Dawei Tang (唐大伟)[*1]

[1)] *Laboratory of Ocean Energy Utilization of Ministry of Education, Dalian University of Technology, Dalian, 116024, China*

[2)] *School of Naval Architecture, Ocean and Civil Engineering, Shanghai Jiao Tong University, Shanghai 200240, China*

[3)] *Department of Ocean Operations and Civil Engineering, Norwegian University of Science and Technology (NTNU), Larsgårdsvegen 2, 6009, Ålesund, Norway*

[4)] *Department of Mechanical and Materials Engineering, Queen's University, Kingston, Ontario K7M 3N9, Canada*

[5)] *School of Engineering, Westlake University, Hangzhou, Zhejiang 310024, China*

[6)] *MIT Sea Grant College Program, Massachusetts Institute of Technology, Cambridge, MA 02139, USA*

[7)] *Massachusetts Institute of Technology, Cambridge, Massachusetts 02139, USA*

(*Electronic mail: dwtang@dlut.edu.cn)

(*Electronic mail: dixia.fan@queensu.ca)

(Dated: 13 November 2022)

As one of the fundamental problems in fluid mechanics, the flow-induced vibration (FIV) of a flexible cylinder helps shed light on various complex fluid-structure interaction (FSI) phenomena, such as the coupling effect of the cross-flow and in-line motions the relationship between external fluid forces and vortical wake patterns. This paper devised a non-uniform in-flow condition (partially uniform flow and partially still water) for flexible cylinders in experimental and numerical conditions. Consistently, a new phenomenon is observed in different scale experiments and simulations that secondary traveling wave vibration of the flexible cylinder is excited from the still water part to the uniform inflow part due to the positive external fluid energy input in the still water. Furthermore, the detailed flow visualization on the vortical wake patterns around the vibrating flexible cylinders reveals that the external fluid force sources in the still water are due to the existence of the attached vortex pair with an uneven strength, which has been observed before in the still rigid cylinder in the oscillatory flow or the rigid cylinder oscillating in the still water at Keulegan–Carpenter (KC) number from 4 to 7.

I. INTRODUCTION

Due to the unstable shedding vortices, long slender structures in ocean current, such as risers, cables, and hawsers, are subject to vibrations. It is referred to as vortex-induced vibrations (VIVs) that may cause the structures unpredictable fatigue damage. Therefore it has attracted a significant amount of research attention over the past decades[3–8].

Flexible cylinders in the non-uniform current exhibit a more complicated spatial distribution of structural vibrations and vortical wake patterns compared to rigid cylinder VIVs[9]. For example, the flexible cylinder response in the highly sheared flow is more likely to show multi-mode, non-"lock-in" behavior than that in mildly sheared conditions[10–12]. Standing waves dominate the VIV response of a rigid cylinder in uniform current, while significant traveling wave responses[13–15] could be observed on the long flexible cylinder in large scale field experiments[16].

Over the past decades, various numerical methods have been proposed to simulate this nonlinear VIVs problem[3]. Among them, the high-fidelity CFD method shows a great advantage in revealing the vortical wake topology[17], even though the computational cost is too high to be applied to industrial applications. To this end, empirical prediction tools still dominate the offshore structure's VIV design[18–20].

In oceans, especially of the water column over 1000m deep, the uniform current is not realistic and seldom met[21]. Typically, the higher velocity current is found close to the surface, and it decreases to a lower or even a zero value in the significant part of the water column[22]. Therefore, the non-uniform current could result in a VIV scenario that the top part of the flexible cylinder vibrates in the current of higher velocity, while the other part of the cylinder vibrates in the current of lower speed or even in the still water.

The vibrating cylinder in still water or cylinder in oscillatory flow has attracted far less attention. Notably, the experiment on rigid cylinder in oscillatory flow performed by Sarpkaya[23] showed that the drag (C_d) and added mass coefficient (C_m) are in tune with the theory: for smooth cylinders, under the critical $KC = 2\pi\frac{A}{d}$ number, the flow transited into unstable state depending on

different $\beta = \frac{fd^2}{\nu}$, where A and f is vibration amplitude and frequency, d is the cylinder diameter and ν is the fluid kinematic viscosity. In addition, Williamson[24] studied lift forces (perpendicular to the oscillation direction) on oscillating a circular cylinder in still fluid, which revealed the fact that the appearance of the different harmonics of the oscillation frequency of the lift force depended on KC too. With increasing KC, the flow pattern changed from a pair of attached vortices around the cylinder to multiple-pair shedding vortices. A more comprehensive flow visualization study was carried out by Tatsuno et al.[25] for a broad range of KC from 1.6 to 15 and various β between 5 and 160, and a comprehensive flow regimes map was established, where eight different flow regimes were identified (A*, A, B, C, D, E, F, and G). However, minimal work has been done on the flexible cylinder oscillating in the still water. It was reported by Fu and Wang, et al.[26–28] that the response of flexible cylinder in oscillatory flow at large KCf features an intermittent VIV response with amplitude modulation including three phases: build-up, lock-in and dry-out.

In current work, we will first carry out experimental measurements on the response of a flexible cylinder in stepped current, in other words, partially in the uniform flow and partially in the still water, which is achieved by hiding part of the flexible cylinder in specially designed bucket to block incoming velocity when towing the model. Subsequently, we will perform the high-fidelity simulation to visualize the surrounding vortical wake pattern and get a deep insight into the corresponding VIV.

The rest of the paper is organized as follows: Section II presents the methods and models used in the experiment and simulation. Section III discusses the experimental and numerical results of the different flexible cylinders in stepped current. Section IV summarizes the main findings of the paper. In the Appendix A, additional experimental results are given.

II. MATERIAL AND METHODS

A. Experimental method and models

The uniform flexible cylinder model used in current experiment has a diameter $d = 1.2cm$ and a length $L = 204cm$ (aspect ratio is 170). The model is constructed/molded via urethane rubber (density of $1.38g/cm^3$) with a mass ratio of $m^* = 4.0$ (the ratio between structural mass to displaced fluid mass). In addition, a fishing line is embedded in the center during the molding process to provide sufficient axial stiffness. In the experiment, the effect of the bending stiffness on the model's natural frequency and modal shape is negligible compared to that of the tensions applied. Note that the structural damping of the urethane rubber material is higher than the traditional metal or ABS plastic cylinder model. Nonetheless, the damping ratio of the current flexible model is 8.2%, as obtained from the pluck test in
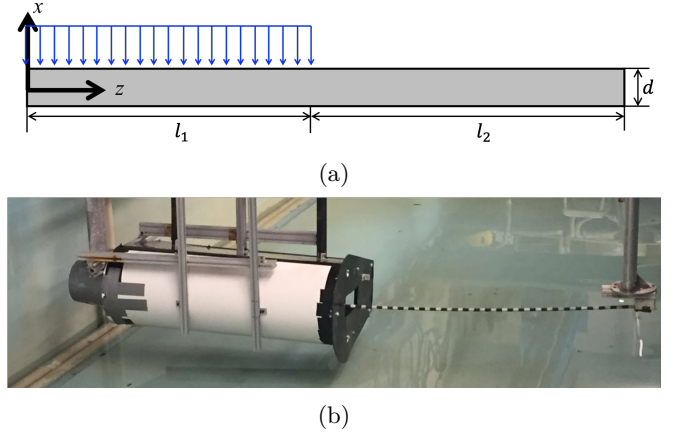

(a)

(b)

FIG. 1: Experimental setup of flexible cylinder half hiding in the still water: a) sketch shows the axis origin and direction; b) photo shows the flexible cylinder setup in the tow tank.

the air. The model properties are shown in Table I labeled as **Exp I**.

Two foil-shaped holders are fixed on the supporting beam in the towing tank, with the model installed on the bottom of the holder that allows tension adjustment. A similar setup has been used in our previous research[29]. To achieve the condition that only part of the flexible cylinder is exposed to the uniform inflow (length of l_2 shown in Fig. 1 (a)) and part of the flexible cylinder (length of l_1 shown in Fig. 1 (a)) responds in the still water, a specially designed bucket is constructed to block the incoming flow, shown in Fig. 1 (b). The top and back of the bucket use the transparent acrylic plate that allows the model's response to be directly observed by the cameras. In addition, a splitting plate is installed in the opening of the bucket to minimize the disturbance of the bucket to the model open-flow part during the towing experiment.

We applied our newly developed underwater optical methods using eight high-speed cameras to capture the Inline (IL) and Cross-flow (CF) vibrations for a total of 46 locations (staggered black and white markers) along the cylinder span. Compared to the traditional strain gauge and accelerometer measurement in flexible cylinder VIV experiments, the optical tracking system provides both temporally and spatially dense and direct measurements on the displacement response[30]. 4 cameras are installed over 80d downstream of the model to measure CF vibration, while six cameras are installed 50d above the model to measure In-Line (IL) vibration. In the meantime, four 1500-lumen underwater lightings are installed to provide enough camera background lighting. Corresponding image processing and motion tracking code have been successfully developed to capture and follow the trajectory of either white or black markers[30,31].

In this paper, the result of the larger-scale flexible cylinder experiment conducted by Chaplin et al. in the

early 2000s[32] is also discussed. Their experiment has been widely used as a benchmark for verification and validation for semi-empirical, and CFD software to predict flexible cylinder VIVs[33]. The experiment was carried out at Delft Hydraulics in the Delta Flume, where the flexible cylinder (total length of 13.12m) passed through the depth of water (6.5m) in the flume and up to the top of a tank (the 'vacuum tank'). The vacuum tank was filled with water by evacuating air during the experiments. When the carriage was moving, the riser thus experienced a stepped current consisting of uniform flow over its lower part and still water over its top part. The model properties are shown in Table I labeled as **Exp II**.
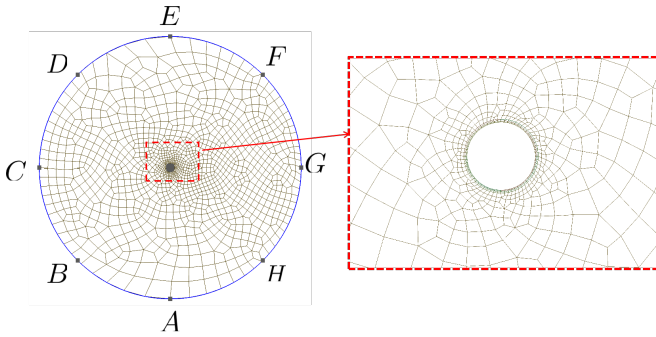
B.   Numerical simulation

FIG. 2: The computational domain and mesh in (x,y) plane: left, mesh of the whole domain, arc $\overset{\frown}{ABCDE}$ is the inflow boundary, arc $\overset{\frown}{EFGHA}$ denotes the outflow boundary; right, mesh structure in the vicinity area around the cylinder.
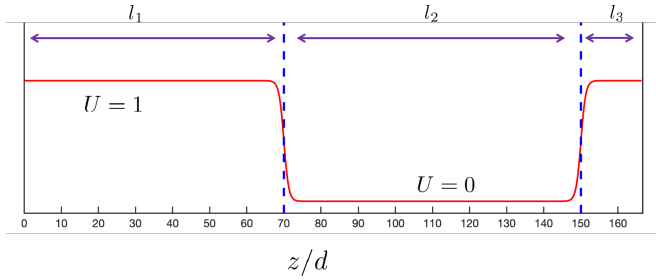

FIG. 3: The stepped inflow velocity profile along z direction. Note that $L = l_1 + l2 = 150\,d$ is the effective inflow region, $l_3 = 16.67\,d$ is the extended "buffer region" in order to recover the periodicity, so that Fourier expansions can be employed along z direction.

Numerical simulation of the vortex-induced vibration of a flexible cylinder in stepped current is rather difficult. To the best of the authors' knowledge, it has scarcely ever been achieved. In this paper, the in-

compressible flow is solved by employing the mixed spectral-element/Fourier method, i.e., spectral-element discretization on the $((x,y))$ plane and Fourier expansion along the cylinder axial direction (z)[34,35]. In particular, the moving boundary due to the vibration is handled by a coordinate transformation method proposed by[36]. Here, the benefit of using the Fourier method is two-fold, as explained in[34]: firstly, the *three-dimensional* flow problem is transformed into a series of *two-dimensional* computations, which can significantly reduce the computing time; secondly, the well-developed FFTW library can be employed to achieve more efficiency. Moreover, the entropy-viscosity method[37–39] based large-eddy simulation (LES) subgrid model is used to take into account the turbulence effect. The computational domain in (x,y) plane is enclosed between two circles, namely $\sqrt{x^2+y^2}=35d$ and $\sqrt{x^2+y^2}=0.5d$, where d is the diameter of the flexible cylinder. As shown in Fig.2, the inflow boundary is placed on arc $\overset{\frown}{ABCDE}$, where velocity is given by $u=U, v=0, w=0$. Here u, v, w are the three components of the velocity vector $\mathbf{u}$. The outflow boundary is on arc $\overset{\frown}{EFGHA}$, where $\frac{\partial \mathbf{u}}{\partial \mathbf{n}}=0$ are prescribed. Note that p is the pressure, and $\mathbf{n}$ is the normal vector. Fig. 3 shows the prescribed inflow velocity profile along the cylinder span. It could be seen that in section $0 \le z \le 70\,d$, $U=1$, while in $70\,d \le z \le 150\,d$, $U=0.0$. The hyperbolic tangential function $\frac{\tanh(\frac{l_1-z}{\eta})+1.0}{2}U$ is used to smooth the stepped inflow velocity from high to low, where η is a constant, whose value is four times of the mesh size in z direction. It is worth noting that although the length of the flexible cylinder is $l_1 + l_2 = 150d$, both the inflow velocity profile and the computational domain are expanded by an additional $16.67d$ to maintain the periodicity in z direction, where the aforementioned hyperbolic tangent function is again used to connect the low velocity ($U=0$) and high velocity ($U=1$) section. The expanded section is named as "buffer region" in[40], which proves that the "buffer region" has negligible impact on the flow and structure vibrations of the rest of the riser, as long as the size of the "buffer region" is small compared to the cylinder length. Furthermore, the domain on the $(x-y)$ plane is partitioned into $2\,320$ quadrilateral elements clustered around the cylinder to resolve the boundary layer. Specifically, on the radial direction, the size of the first layer element around the cylinder is $0.01D$, which gives rise to $y^+ < 1$ in all the simulations of this paper, and along the azimuthal direction, the element edge length is $\frac{\pi d}{64}$.

In this paper, the reduced velocity is defined as,

$$U_r = \frac{U}{f_{n1}d} \qquad (1)$$

where $f_{n1} = \frac{1}{2L}\sqrt{\frac{T}{(m^*+C_m)\frac{\rho_f \pi d^2}{4}}}$ is the first modal natural frequency, where m^* is the cylinder mass ratio, T is the static tension applied on the cylinder, ρ_f is the fluid density, $C_m = 1.0$ is the assumed added mass coefficient.

TABLE I: Nomenclature.

Case	Exp I	Exp II[32]	Sim
Length (L)	2.04m	13.12m	150
Diameter(d)	1.2cm	2.8cm	1
Aspect Ratio (L/d)	170	469	150
Exposure Ratio (l_1/L)	0.5	0.45	0.47
Mass Ratio (m^*)	1.38	3.0	2.55

The flexible cylinder motion is governed by the following equation,

$$\frac{\partial^2 \xi_J}{\partial t^2} + 2\zeta \omega_n \frac{\partial \xi_J}{\partial t} + \frac{EI}{\mu} \frac{\partial^4 \xi_J}{\partial z^4} - \frac{T}{\mu} \frac{\partial^2 \xi_J}{\partial z^2} = \frac{C_J}{2\mu}, \quad (2)$$

where ξ_J is the displacement along the J-direction ($J = x$ or $J = y$), and $\mu = m^* \frac{\rho_f \pi d^2}{4}$ is the cylinder mass per unit length, ζ is the damping coefficient with $\omega_n = 2\pi \frac{U_\infty}{U_r d}$, and EI is the bending stiffness. Note that in the simulation, T is a constant along the cylinder span, and $EI < 10^{-4}$ to ensure that the riser is tension dominated, see[41]. C_J is the J-component of the hydrodynamic force coefficient exerted on the cylinder surface. Eq. 2 is constrained by the pinned boundary condition ($\xi_J = 0$ and $\frac{\partial^2 \xi_J}{\partial z^2} = 0$) at $z/d = 0$ and $z/d = 150$. In the simulation, $m^* = 2.55$, $Ur = 15$, $\zeta = 2.0\%$, and the flow Reynolds number is set as $Re = U d/\nu = 1000$, where ν is the kinematic viscosity. Note that the parameters used in simulation is placed in Table I labeled as **Sim**.

Eq. 2 is discretized by the 2nd order central-difference scheme in space and the Runge-Kutta method in time. Three spectral-element modes in each element on the (x, y) plane, and 512 Fourier planes along the axis (z direction) are employed in the simulation. Note that in order to minimize the aliasing error, we employ over integration, i.e., we use 5-points Gauss-Lobatto quadrature in each element and the 3/2 de-aliasing rule in the Fourier direction. The total computational time $\frac{tU_\infty}{d} \geq 400$ with a time step $\frac{\Delta t U_\infty}{D} = 1.0 \times 10^{-3}$, which results in the CFL number less than 0.3.

III.   RESULT AND DISCUSSION

A.   Structural response in the experiments

We measured the structural response of the flexible cylinder in the range of towing velocities (U) from 0.2 m/s to 0.6 m/s. The results of the two cases of $U = 0.5m/s$ and $U = 0.35m/s$ are presented in this section and in Appendix. Fig. 4 shows the structural response (the displacement A is defined as A_x for the IL direction and A_y for the CF direction.) along the flexible cylinder at $U = 0.5m/s$ of **Exp I**: the CF frequency response, the IL frequency response, the displacement response in both directions and phase response of the CF 1st, IL 1st and the
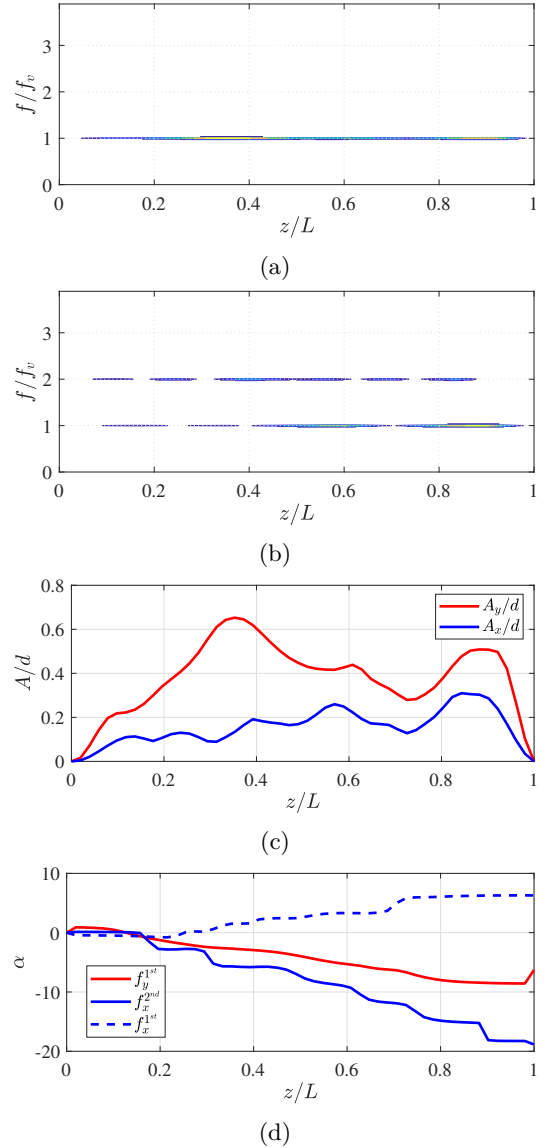

FIG. 4: Structural response along the flexible cylinder at $U = 0.5m/s$ of **Exp I**: (a) the CF frequency response along the model span, normalized by the peak CF vibration frequency $f_v = 7.70$; (b) the IL frequency response along the cylinder span, normalized by the peak CF vibration frequency $f_v = 7.70$; (c) the standard deviation of the CF and the IL displacement response along the cylinder span; (d) the phase response of the CF 1st, IL 1st and the 2nd harmonics along the cylinder span.

2nd harmonics along the flexible model are plotted in Fig. 4 (a) - (d) respectively. Among them, the power spectral density (PSD) analysis of the CF and the IL frequency response in Fig. 4 (a) and (b) shows that the flexible cylinder responds in a narrow-banded single frequency in the CF direction, while both the 2nd harmonics and a strong 1st harmonics appears in the IL direction of the flexible cylinder. In our previous experiment on a tension domi-

(a)

(b)

(c)

(d)
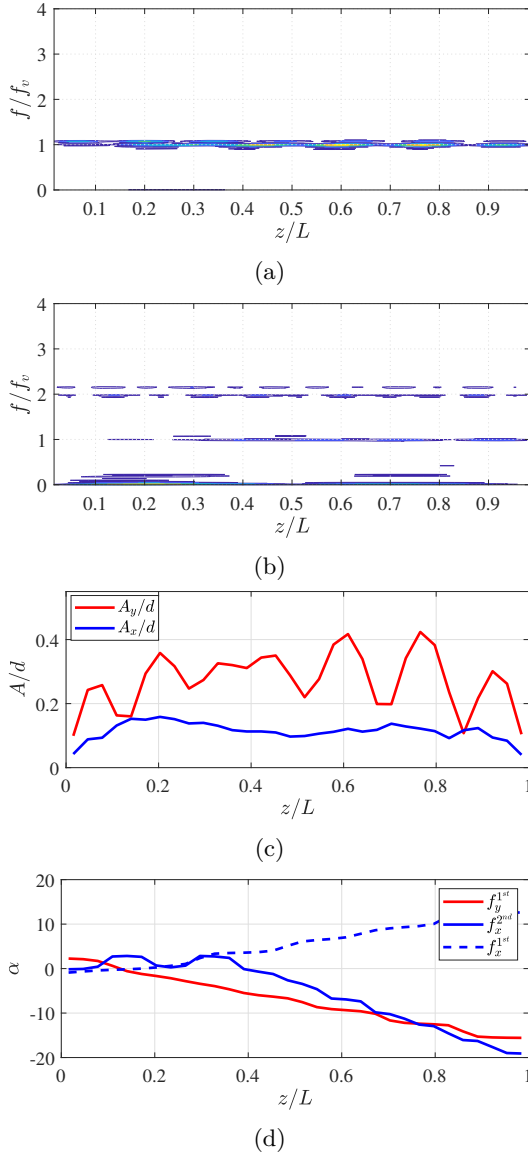
FIG. 5: Structural response along the flexible model at $U = 0.65 m/s$ (case 21A012) in **Exp II**[32]: (a) the CF frequency response along the model span, normalized by the peak CF vibration frequency $f_v = 4.06 Hz$; (b) the IL frequency response along the model span, normalized by the peak CF vibration frequency $f_v = 4.06 Hz$; (c) the standard deviation of the CF and the IL displacement response along the model span; (d) the phase response of the CF 1st, IL 1st and the 2nd harmonics along the model span.

FIG. 6: Structural response along the flexible model at $U_r = 15$ and **Re** $= 1,000$ in the simulation: (a) the CF frequency response along the model span, normalized by the peak CF vibration frequency $f_v = 0.201$; (b) the IL frequency response along the model span, normalized by the peak CF vibration frequency $f_v = 0.201$; (c) the standard deviation of the CF and the IL displacement response along the model span; (d) the phase response of the CF 1st, IL 1st and the 2nd harmonics along the model span.

nated flexible cylinder in uniform flow, normally the displacement response is a single narrow-banded single frequency of the 2nd harmonics in the IL direction[17,42,43].In addition, the displacement in both directions is shown Fig. 4 (c). Calculating the phase between the imaginary and real parts of the Fourier expansions of the displacement along the cylinder span, the phase responses of the
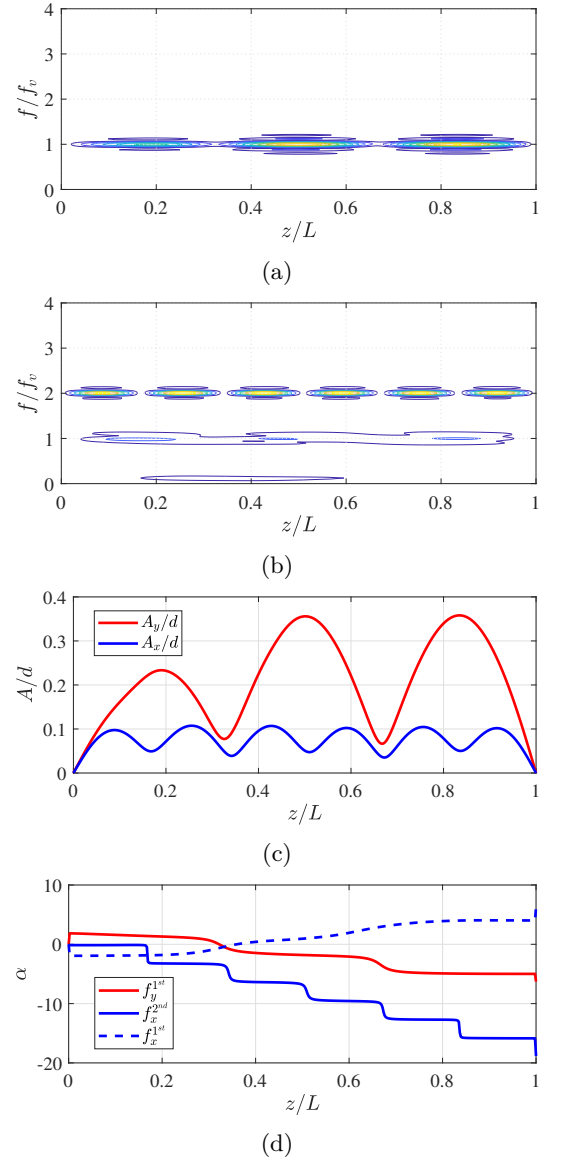
CF 1st, the IL 1st and the IL 2nd harmonics are plotted in Fig. 4 (d). It is found that the CF 1st and the IL 2nd harmonics respond in a traveling pattern from $z/L = 0$ to $z/L = 1$, corresponding to from open flow part to still water part, while the IL 1st harmonic vibration component travels from $z/L = 1$ to $z/L = 0$, corresponding to from still water part to open flow part.
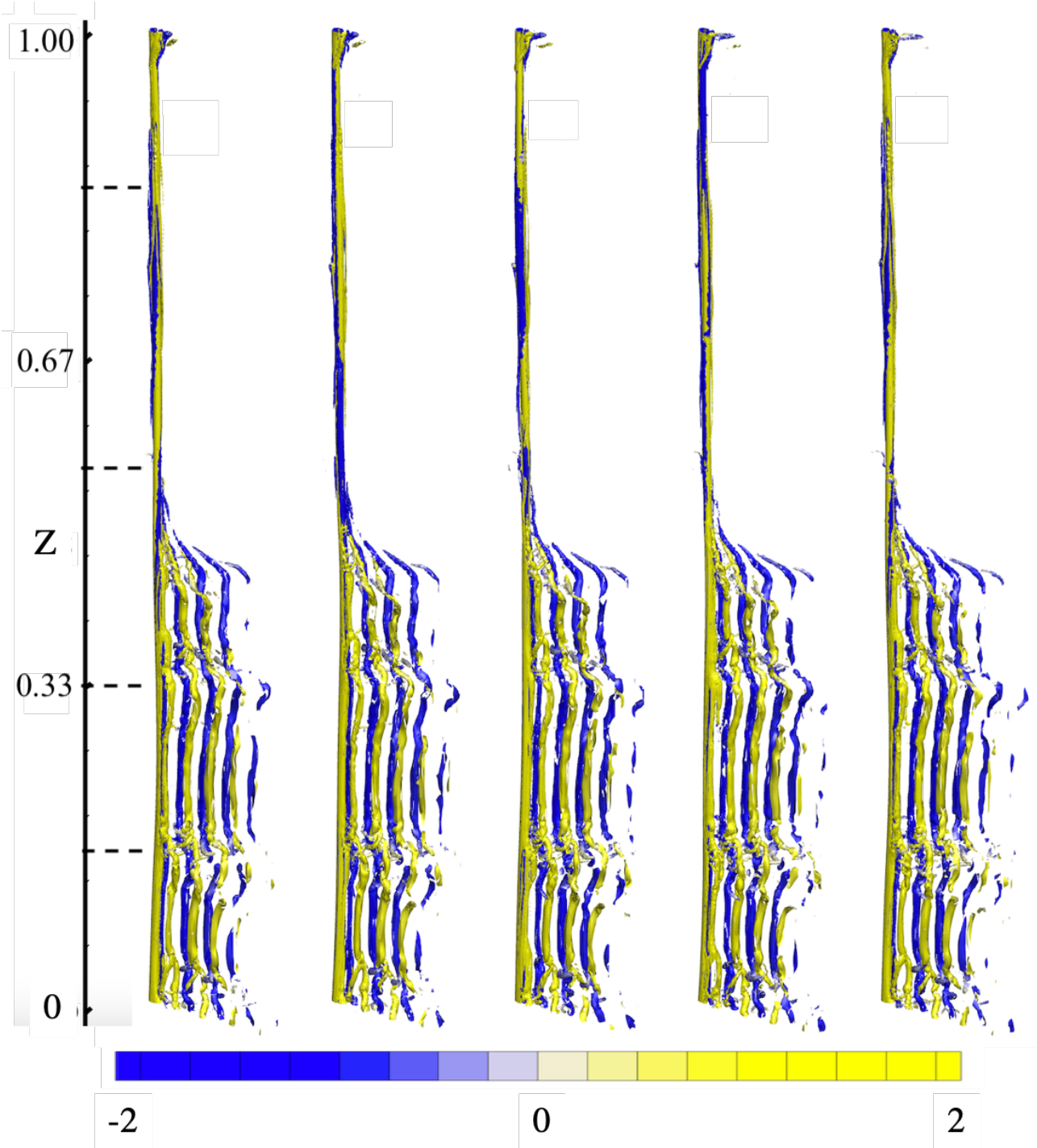
FIG. 7: 3D Vortices from the simulation of a flexible cylinder at $U_r = 15$ and $Re = 1,000$. From left to right, the time snapshots are $t_r = \frac{tU}{d}$: 3.75, 4.875, 6.125, 7.375 and 8.625, corresponding to black dashed line in the sub-figure (d) of Fig. 8, Fig. 9, Fig. 10 and Fig. 11. Here vortices are represented by iso-surfaces of $Q = 0.2$ and colored by ω_z.

As shown above, the interesting phenomenon that strong 1st IL harmonic vibration travels from the cylinder section in still water to that in open flow, there might be an external disturbance source that can transfer energy from fluid to structure in the still water in the IL direction. Note that the same phenomenon has also been observed and reported by Chaplin et al.[32]. The result of the experiment on the 13.16m flexible cylinder at $U = 0.65 m/s$ denoted by case 21A012 shows a similar phenomenon, see Fig. 5 (a) - (d). In particular, Fig. 5 (a) and (b) show that apart from the 2nd harmonics in the IL direction, there is a strong 1st vibration harmonics
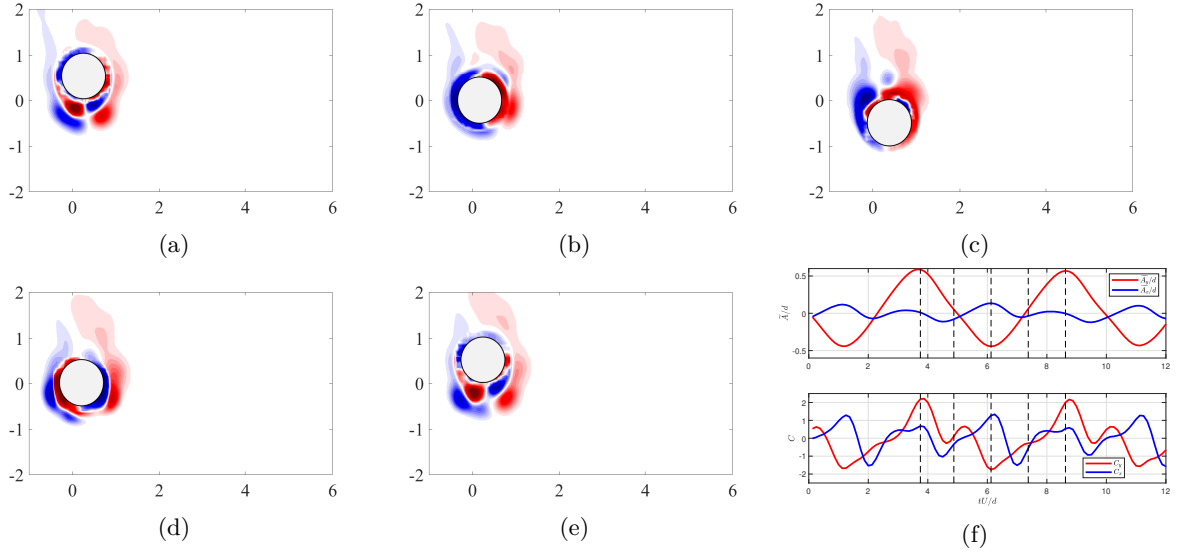
FIG. 8: Snapshots of two-dimensional vortex at location of the cylinder $z/L = 0.867$ at $t = 0$ (a), $t = \frac{T}{4}$ (b), $t = \frac{T}{2}$ (c), $t = \frac{3T}{4}$ (d) and $t = T$ (e), as well as the corresponding motion and force (f).
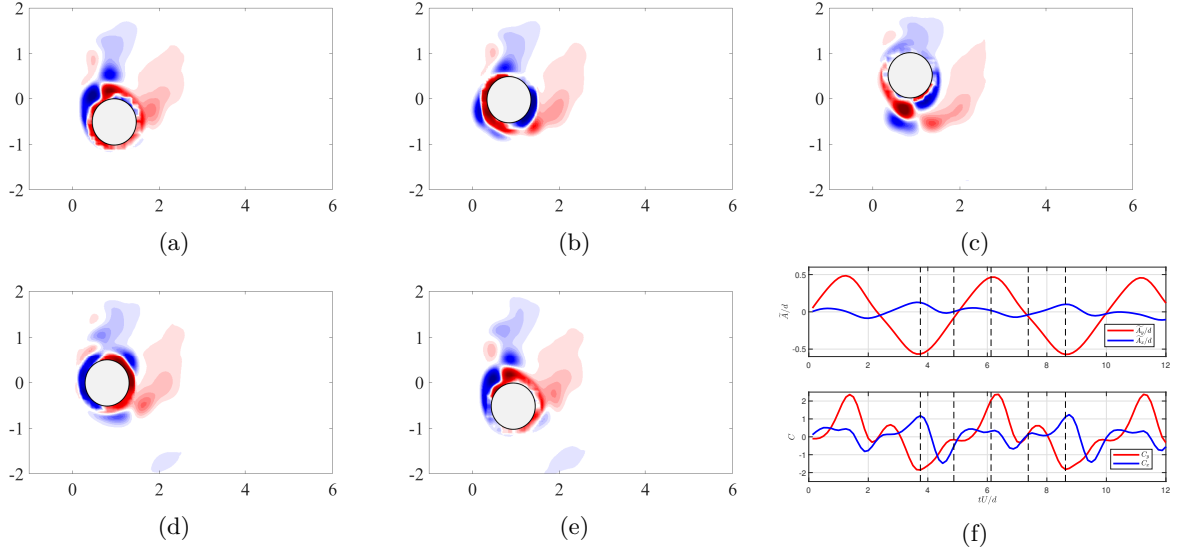

FIG. 9: Snapshots of two-dimensional vortex at location of the cylinder $z/L = 0.533$ at $t = 0$ (a), $t = \frac{T}{4}$ (b), $t = \frac{T}{2}$ (c), $t = \frac{3T}{4}$ (d) and $t = T$ (e), as well as the corresponding motion and force (f).

in the IL direction as well and Fig. 5 (d) shows that the 1st IL vibration harmonics travels a different direction from still water part to open flow part, opposite from the 1st CF vibration and the 2nd IL vibration harmonics.

It should be noted that the hypothesis of an external fluid disturbance source in the still water inducing the 1st IL vibration maybe not be correct. This IL vibration response could be due to the structural coupling effect between flexible cylinder CF and IL response in the experiment, as the flexible model is twisted in the installation.

B. Vortical wake visualization in simulation

To determine whether an external fluid disturbance source in the still water exists, LES is performed on an IL and CF coupled flexible cylinder in stepped current to visualize the shedding vortices.

Here the response of the flexible cylinder with 47% of its length in the uniform flow at $U_r = 15$ and $Re = 1,000$ is given in Fig. 6 (a) to (d). The result is similar to those found in **Exp I** and **Exp II** that there is a strong 1st harmonic vibration component in the IL direction traveling from the part of the cylinder part in still water to
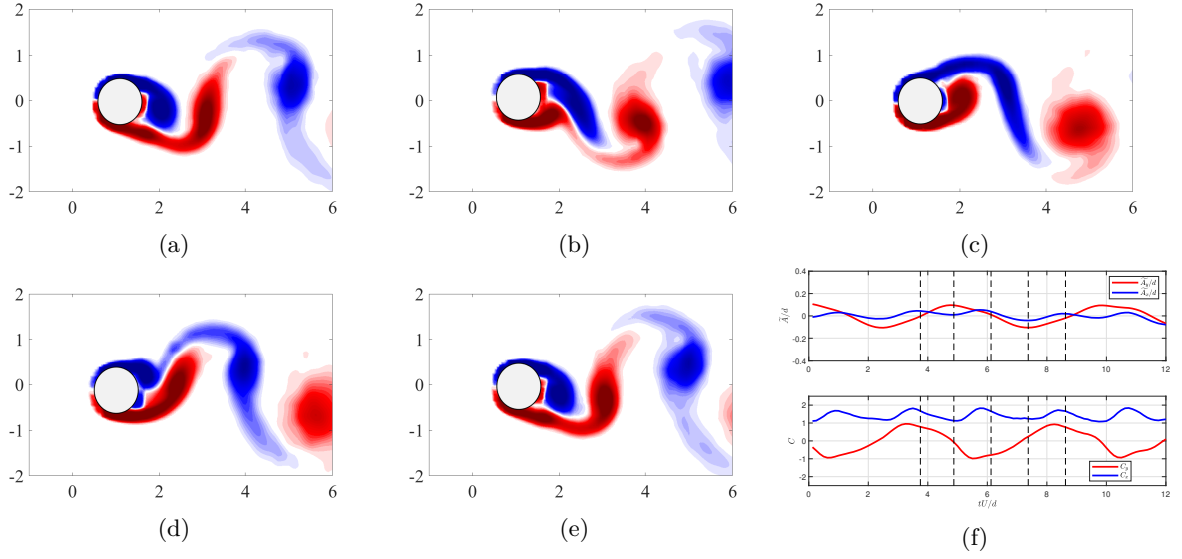
FIG. 10: Snapshots of two-dimensional vortex at location of the cylinder $z/L = 0.333$ at $t = 0$ (a), $t = \frac{T}{4}$ (b), $t = \frac{T}{2}$ (c), $t = \frac{3T}{4}$ (d) and $t = T$ (e), as well as the corresponding motion and force (f).
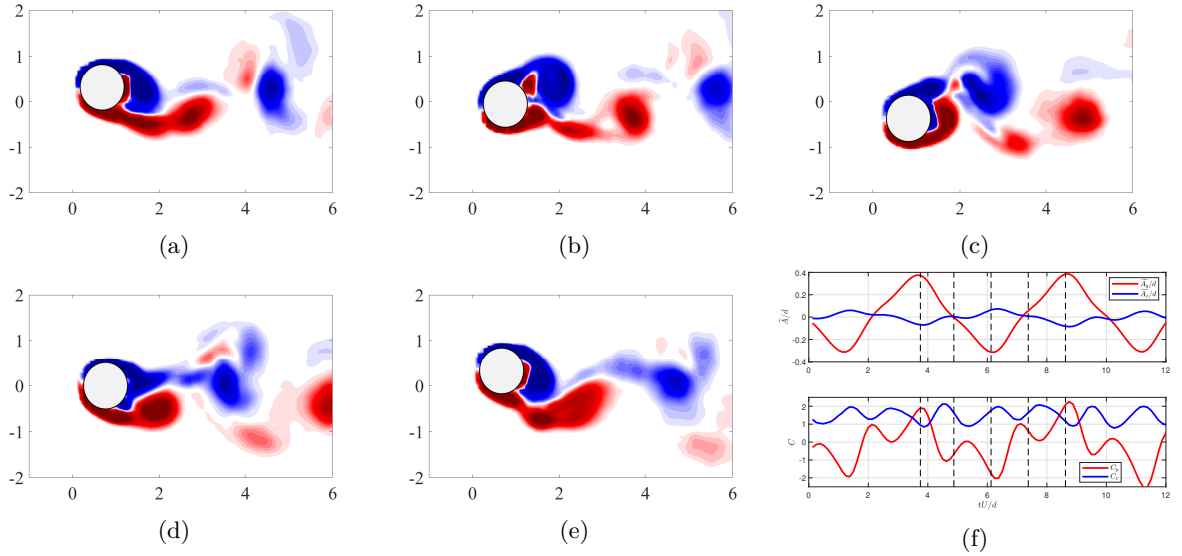

FIG. 11: Snapshots of two-dimensional vortex at location of the cylinder $z/L = 0.167$ at $t = 0$ (a), $t = \frac{T}{4}$ (b), $t = \frac{T}{2}$ (c), $t = \frac{3T}{4}$ (d) and $t = T$ (e), as well as the corresponding motion and force (f).

that in open flow, in the opposite direction to the 1st harmonic vibration component in the CF direction and the 2nd harmonic vibration component in the IL direction. The simulation result further demonstrates that the induced strong 1st harmonic vibration component in the IL direction is a result of external fluid source, it is not due to the IL and CF structural coupling effect because of the imperfect experimental installation.

A vortical flow pattern analysis is performed to understand better the mechanisms of interaction between the fluid and the structure. The snapshots of the 3D wake visualization obtained from the LES of the flexible cylin-

der at $U_r = 15$ and $Re = 1,000$ at five-time instants are plotted in Fig. 7. In the lower part of the cylinder that is subject to uniform inflow, it could be observed that the IL nodes can separate the vortex tube formation behind the cylinder into different cells alternatively distributed along the spanwise direction. A similar phenomenon has been identified and explained in detail in our previous experimental and simulation work on the flexible cylinder in the uniform flow[17,44]. Differently, in the upper still water region, it could be seen that the vortex tube is attached to the vibrating flexible cylinder with an alternating sign of vorticity.

To visualize the relative motion between the local shedding vortex and oscillating cylinder, the snapshots of *two dimensional* vortex at four locations of the cylinder, namely $z/L = 0.867$, $z/L = 0.533$, $z/L = 0.333$ and $z/L = 0.167$, as well as the corresponding motion and force are plotted in Fig. 8 to Fig. 11. It could be observed that in the still water region, see Fig. 8 and Fig. 9 (a) to (e), these cylinder sections oscillate in the Y direction (corresponding to the CF direction in the uniform open flow region) with an attached vortex pair of unequal strength. These asymmetric vortex pairs do not form simultaneously, upon flow reversal, which gives rise to an oscillatory force perpendicular to the main oscillation direction, at the main oscillation frequency, as shown in Fig. 8 (f) and Fig. 9 (f). Note that a similar phenomenon was first reported by Williamson[24], where the rigid cylinder in the oscillatory flow in the region of $KC = 2\pi\frac{A}{d} < 7$, which is in the attached vortex pair regime, a vortex pair of an unequal strength will give rise to the "a lift force of low amplitude fluctuating at the oscillation frequency"[24].

Therefore, the mechanism of the observed phenomenon in both the experiment and simulation can be explained as follows: the continuously alternating vortex shedding from the flexible cylinder in the uniform open flow results in a steady vibration of 1st harmonics in the CF direction with an amplitude close to 0.5 - 1 diameter and the 2nd harmonics in the IL direction with a small amplitude. These vibration components hence travel from the cylinder section in open flow to that in the still water. If the oscillation in the still water is in $KC \in [4,7]$ ($A/d \in [0.5,1]$), it gives rise to oscillatory force in the IL direction with the same 1st harmonic frequency, which in turn results in a 1st harmonic vibration component in the IL direction traveling back from still water to the open flow.

IV. CONCLUSION

In this paper, we reported for the first time, both experimentally and numerically, a new phenomenon of secondary traveling wave vibration in the IL direction of the flexible cylinder when the flexible cylinder is placed partially in the uniform inflow and partially in the still water. It is a universal phenomenon that could be found in different flexible cylinder experiments and simulations of various scales. The phenomenon is characterized by 1) same as that of the traditional flexible cylinder, VIV of 1st CF harmonics and the 2nd IL harmonics vibration were excited in the uniform inflow region, but 2) the unconventional external disturbance (positive energy-in) in the still water region generates the strong 1st IL harmonic vibration traveling from the still water region to uniform inflow region. A high-fidelity simulation was conducted to visualize the vortical wake around the vibrating flexible cylinder in both the uniform flow and still water regions, in order to figure out the fluid-structure interac-

tion mechanism. The flow visualization reveals that the attached vortex pair around the flexible cylinder oscillating in the still water will give rise to an oscillatory force perpendicular to the CF direction at the main oscillation frequency, which results in the strong IL vibration of 1st harmonics traveling from the still water region to uniform inflow region.

Appendix A: Additional experimental cases

Two additional experimental cases of $U = 0.35 m/s$ in Exp I and $U = 0.95 m/s$ (case 21A018) in Exp II are shown in Fig. 12 and Fig. 13.

DATA AVAILABILITY STATEMENT

The data that support the findings of this study are available within the article

[1+] Equally contributed first authors.
[2*] Corresponding authors.
[3] R. D. Gabbai and H. Benaroya, "An overview of modeling and experiments of vortex-induced vibration of circular cylinders," J. Sound Vib. **282**, 575–616 (2005).
[4] C. H. K. Williamson and R. Govardhan, "A brief review of recent results in vortex-induced vibrations," J. Wind Eng. and Ind. Aero. **96**, 713–735 (2008).
[5] X. Huang, H. Zhang, and X. Wang, "An overview on the study of vortex-induced vibration of marine riser," Journal of marine sciences **27**, 95–101 (2009).
[6] P. W. Bearman, "Circular cylinder wakes and vortex-induced vibrations," J. Fluids Struct. **27**, 648–658 (2011).
[7] X. Wu, F. Ge, and Y. Hong, "A review of recent studies on vortex-induced vibrations of long slender cylinders," Journal of Fluids and Structures **28**, 292–308 (2012).
[8] J. Wang, D. Fan, and K. Lin, "A review on flow-induced vibration of offshore circular cylinders," Journal of Hydrodynamics **32**, 415–440 (2020).
[9] J. M. Dahl, *Vortex-induced vibration of a circular cylinder with combined in-line and cross-flow motion*, Ph.D. thesis, Massachusetts Institute of Technology (2008).
[10] J. K. Vandiver, D. Allen, and L. Li, "The occurrence of lock-in under highly sheared conditions," Journal of Fluids and Structures **10**, 555–561 (1996).
[11] W.-L. Chen, Q.-Q. Zhang, H. Li, and H. Hu, "An experimental investigation on vortex induced vibration of a flexible inclined cable under a shear flow," Journal of Fluids and Structures **54**, 297–311 (2015).
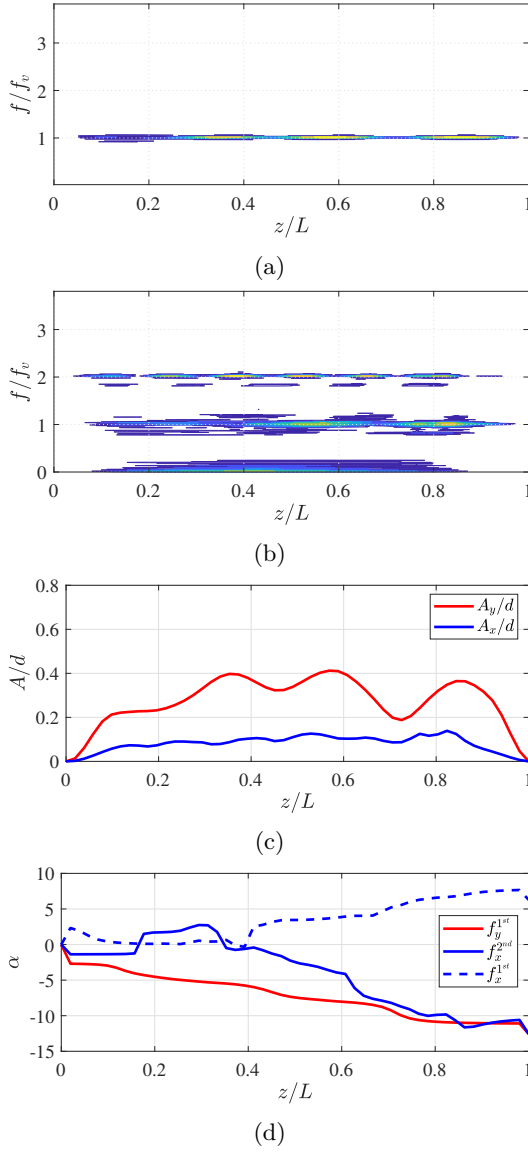
(a)

(b)

(c)

(d)

FIG. 12: Structural response along the flexible cylinder at $U = 0.35 m/s$ in **Exp I**: (a) the CF frequency response along the model span, normalized by the peak CF vibration frequency $f_v = 5.91$; (b) the IL frequency response along the model span, normalized by the peak CF vibration frequency $f_v = 5.91$; (c) the standard deviation of the CF and the IL displacement response along the model span; (d) the phase response of the CF 1st, IL 1st and 2nd harmonics along the model span.
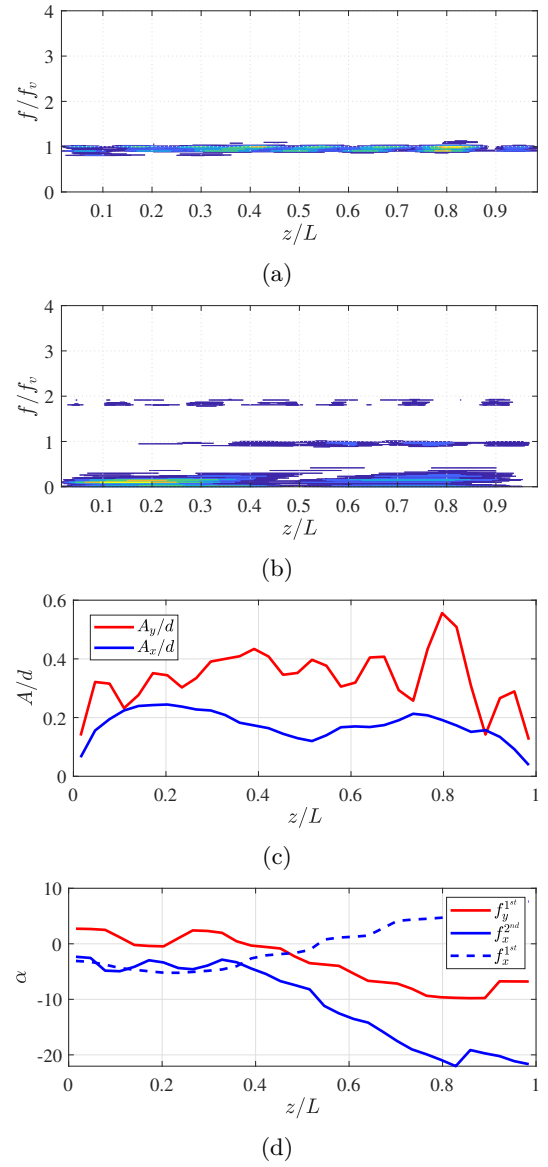
FIG. 13: Structural response along the flexible cylinder at $U = 0.95 m/s$ (case 21A018) in **Exp II**[32]: (a) the CF frequency response along the model span, normalized by the peak CF vibration frequency $f_v = 5.78 Hz$; (b) the IL frequency response along the model span, normalized by the peak CF vibration frequency $f_v = 5.78 Hz$; (c) the standard deviation of the CF and the IL displacement response along the model span; (d) the phase response of the CF 1st, IL 1st and the 2nd harmonics along the model span.

[12]C. Ji, Y. Hua, D. Xu, G. Xing, and W. Chen, "Numerical simulation of vortex-induced vibration of a flexible cylinder exposed to shear flow at different shear rates," Chinese Journal of Theoretical and Applied Mechanics **50**, 21 (2018).

[13]J. Wu, H. Lie, C. M. Larsen, S. Liapis, and R. Baarholm, "Vortex-induced vibration of a flexible cylinder: interaction of the in-line and cross-flow responses," J. Fluids Struct. **63**, 238–258 (2016).

[14]E. D. Gedikli, D. Chelidze, and J. M. Dahl, "Observed mode shape effects on the vortex-induced vibration of bending domi-

nated flexible cylinders simply supported at both ends," Journal of Fluids and Structures **81**, 399–417 (2018).

[15]Z.-S. Chen and S. H. Rhee, "Effect of traveling wave on the vortex-induced vibration of a long flexible pipe," Applied Ocean Research **84**, 122–132 (2019).

[16]J. K. Vandiver, V. Jaiswal, and V. Jhingran, "Insights on vortex-induced, traveling waves on long risers," Journal of fluids and structures **25**, 641–653 (2009).

[17] D. Fan, Z. Wang, M. S. Triantafyllou, and G. E. Karniadakis, "Mapping the properties of the vortex-induced vibrations of flexible cylinders in uniform oncoming flow," Journal of Fluid Mechanics **881**, 815–858 (2019).

[18] P. Voie, J. Wu, T. L. Resvanis, C. M. Larsen, J. K. Vandiver, M. Triantafyllou, and R. Baarholm, "Consolidation of empirics for calculation of viv response," in *International Conference on Offshore Mechanics and Arctic Engineering*, Vol. 57649 (American Society of Mechanical Engineers, 2017) p. V002T08A031.

[19] M. S. Triantafyllou, G. S. Triantafyllou, Y. S. Tein, and B. D. Ambrose, "Pragmatic riser viv analysis," in *Offshore Tech. Conf* (Offshore Technology Conference, 1999).

[20] C. M. Larsen, K. Vikestad, R. Yttervik, E. Passano, and G. S. Baarholm, "Vivana theory manual," Marintek, Trondheim, Norway (2001).

[21] L. K. Shay, R. L. Elsberry, and P. G. Black, "Vertical structure of the ocean current response to a hurricane," Journal of physical oceanography **19**, 649–669 (1989).

[22] R. Bourguet, G. E. Karniadakis, and M. S. Triantafyllou, "Distributed lock-in drives broadband vortex-induced vibrations of a long flexible cylinder in shear flow," J. Fluid Mech. **717**, 361–375 (2013).

[23] T. Sarpkaya, "Force on a circular cylinder in viscous oscillatory flow at low keulegan—carpenter numbers," Journal of Fluid Mechanics **165**, 61–71 (1986).

[24] C. Williamson, "Sinusoidal flow relative to circular cylinders," Journal of Fluid Mechanics **155**, 141–174 (1985).

[25] M. Tatsuno and P. Bearman, "A visual study of the flow around an oscillating circular cylinder at low keulegan–carpenter numbers and low stokes numbers," Journal of Fluid Mechanics **211**, 157–182 (1990).

[26] S. Fu, J. Wang, R. Baarholm, J. Wu, and C. Larsen, "Features of vortex-induced vibration in oscillatory flow," Journal of Offshore Mechanics and Arctic Engineering **136** (2014).

[27] J. Wang, S. Xiang, S. Fu, P. Cao, J. Yang, and J. He, "Experimental investigation on the dynamic responses of a free-hanging water intake riser under vessel motion," Marine Structures **50**, 1–19 (2016).

[28] J. Wang, S. Fu, J. Wang, H. Li, and M. C. Ong, "Experimental investigation on vortex-induced vibration of a free-hanging riser under vessel motion and uniform current," Journal of Offshore Mechanics and Arctic Engineering **139** (2017).

[29] D. Fan and M. S. Triantafyllou, "Vortex-induced vibration of riser with low span to diameter ratio buoyancy modules," in *The 27th Inter. Offshore and Polar Eng. Conf* (International Society of Offshore and Polar Engineers, 2017).

[30] D. Fan, H. Du, and M. S. Triantafyllou, "Optical tracking measurement on vortex-induced vibration of flexible riser with short-length buoyance module," in *APS Fluid Dyn. Meeting Abstr* (2016).

[31] D. Fan, B. Wu, D. Bachina, and M. S. Triantafyllou, "Vortex-induced vibration of a piggyback pipeline half buried in the seabed," Journal of Sound and Vibration **449**, 182–195 (2019).

[32] J. R. Chaplin, P. W. Bearman, F. J. Huera-Huarte, and R. J. Pattenden, "Laboratory measurements of vortex-induced vibrations of a vertical tension riser in a stepped current," J. Fluids Struct. **21**, 3–24 (2005).

[33] J. R. Chaplin, P. W. Bearman, Y. Cheng, E. Fontaine, J. M. R. Graham, K. Herfjord, F. J. Huera-Huarte, M. Isherwood, K. Lambrakos, C. M. Larsen, *et al.*, "Blind predictions of laboratory measurements of vortex-induced vibrations of a tension riser," J. Fluids Struct. **21**, 25–40 (2005).

[34] G. Karniadakis and S. Sherwin, *Spectral/hp element methods for computational fluid dynamics* (Oxford University Press, 2013).

[35] D. J. Newman and G. E. Karniadakis, "Simulations of flow over a flexible cable: a comparison of forced and flow-induced vibration," J. Fluids Struct. **10**, 439–453 (1996).

[36] D. J. Newman and G. E. Karniadakis, "A direct numerical simulation study of flow past a freely vibrating cable," J. Fluid Mech. **344**, 95–136 (1997).

[37] J.-L. Guermond, R. Pasquetti, and B. Popov, "Entropy viscosity method for nonlinear conservation laws," Journal of Computational Physics **230**, 4248–4267 (2011).

[38] J.-L. Guermond, R. Pasquetti, and B. Popov, "From suitable weak solutions to entropy viscosity," in *Quality and Reliability of Large-Eddy Simulations II* (Springer, 2011) pp. 373–390.

[39] Z. Wang, M. S. Triantafyllou, Y. Constantinides, and G. E. Karniadakis, "A spectral-element/fourier smoothed profile method for large-eddy simulations of complex viv problems," Computers & Fluids **172**, 84–96 (2018).

[40] R. Bourguet, G. E. Karniadakis, and M. S. Triantafyllou, "Vortex-induced vibrations of a long flexible cylinder in shear flow," Journal of fluid mechanics **677**, 342–382 (2011).

[41] C. Evangelinos and G. E. Karniadakis, "Dynamics and flow structures in the turbulent wake of rigid and flexible cylinders subject to vortex-induced vibrations," J. Fluid Mech. **400**, 91–124 (1999).

[42] Z. Wang, D. Fan, M. S. Triantafyllou, and G. E. Karniadakis, "A large-eddy simulation study on the similarity between free vibrations of a flexible cylinder and forced vibrations of a rigid cylinder," Journal of Fluids and Structures **101**, 103223 (2021).

[43] Z. Wang, D. Fan, and M. S. Triantafyllou, "Illuminating the complex role of the added mass during vortex induced vibration," Physics of Fluids **33**, 085120 (2021).

[44] Z. A. Bangash and F. J. Huera-Huarte, "On the flow around the node to anti-node transition of a flexible cylinder undergoing vortex-induced vibrations," Physics of Fluids **27**, 065112 (2015).